

# The 2D Organic Topological Insulators $T(C_6H_5)_3$ ( $T = V, Mn, Fe, Tc, Re$ )

FENGDONG LV, FEI FENG, FANFAN SHANG, QIANG CHUAI AND GUANGTAO WANG\*

College of Physics, Henan Normal University, Xinxiang, Henan 453007, China

(Received December 30, 2019; in final form February 25, 2020)

The quantum anomalous Hall effect will play a special role in electronic devices in the future. It can be used to manufacture electronic devices with low energy consumption and high speed, so as to promote the progress of information technology. We obtain some properties of the two-dimensional organic material  $T(C_6H_5)_3$  ( $T = V, Mn, Fe, Tc, Re$ ) by first-principles calculations. We find that the 2D organic material is a Dirac semimetal in the absence of spin-orbit coupling. When the spin-orbit coupling is included, the Dirac semimetal will evolve into a topological insulator with a quantum anomalous Hall effect. Our work provides a platform to realize topological insulators in the two-dimensional organic.

DOI: [10.12693/APhysPolA.137.1158](https://doi.org/10.12693/APhysPolA.137.1158)

PACS/topics: 2D organic material, Dirac semimetal, topological insulator

## 1. Introduction

The quantum anomalous Hall effect (QAHE) state was proposed by Haldane in 1988 in a 2D lattice model with spontaneous time-reversal symmetry breaking [1]. However, there was no material or specific physical method to realize the QAHE for many years. In 2008, Zhang et al. pointed out a new way to realize the QAHE in magnetic ions doped topological insulators [2–5]. In 2010, Fang et al. innovatively proposed that  $Bi_2Te_3$ ,  $Bi_2Se_3$ , and  $Sb_2Te_3$  topological insulators doped with Cr or Fe magnetic ions can form stable ferromagnetic insulators, which are the best systems to achieve the QAHE [6]. In 2013, Xue et al. observed the QAHE for the first time in experiments [7]. In 2004, the synthesis of graphene marked the rapid development of two-dimensional materials [8]. After that, graphene attracted the interest of the scientific community with its amazing properties. It has been proposed that the QAHE in graphene could be achieved by introducing the Rashba spin-orbit coupling [9, 10]. However, it is extremely difficult to realize the QAHE on graphene because of its very small spin-orbit coupling (SOC) strength. Therefore, we have to search for new materials that can more easily realize QAHE in experiments.

So far, a large number of 2D materials with QAHE have been theoretically predicted, such as 2D oxides [11–13], 2D cyanide [14, 15], and the Kagome lattice ferromagnet [16]. In addition, several 2D organic molecules with hexagonal organometallic frameworks (HOMFs) connected by metal atoms have also been developed rapidly [17–19]. These organometallic compounds can be synthesized by self-organized growth on special substrate [20–21]. The chiral edge states associated with quantum Hall conductance are topologically

protected. These interesting properties provide potential applications for future nanoelectronics and integrated circuit. In general, organic materials have more advantages, such as low cost, ease of manufacturing, and mechanical flexibility, compared to inorganic materials. Many traditional inorganic materials and devices have been replaced by organic materials, such as organic superconductors [22], light-emitting diodes [23], solar cells [24], and field-effect transistors [25]. Such new organic materials also have broad applications in biomedical field [26], catalysis [27], drug delivery [28], and gas storage [29]. The QAHE has been observed in Cr doped  $(Bi,Sb)_2Te_3$  films in recent years [30–32].

With the continuous development of synthetic chemistry and nanotechnology, scientists have predicted and prepared more and more two-dimensional organic topological insulators [33–37]. Two-dimensional organic topological insulators also have band inversion caused by spin-orbit coupling and topological boundary states of connected valence bands and conduction bands, similar to the properties of 2D inorganic topological insulators. Since the type of 2D inorganic topological insulator is limited by crystal symmetry and atomic orbital, the number is limited. For two-dimensional metal-organic materials, there are many kinds of organic molecules in 2D organometallic materials, and there may be more two-dimensional organic topological insulators. The coordination between organic molecules and metal atoms makes it possible to have more magnetic 2D topological insulators that can realize the QAHE. At the same time, the research of 2D organic topological insulators further expand the organic materials in the application of spintronics which have stimulated the interest of scientists [38–40]. It is important to synthesize very stable and easily synthesizable 2D topological insulators. It can realize the QAHE without external magnetic field and reduce dissipation. The application of 2D topological insulators will bring about another semiconductor revolution. Here, we introduce the 2D organic topological

\*corresponding author; e-mail: [fedolv@163.com](mailto:fedolv@163.com)

insulator  $T(\text{C}_6\text{H}_5)_3$  ( $T = \text{V}, \text{Mn}, \text{Fe}, \text{Tc}, \text{Re}$ ). We predict that it is a kind of material that can realize the QAHE. In addition, materials with similar structure have been synthesized experimentally [41]. These materials have a hexagonal symmetrical structure. In such materials, metal atoms form a hexagonal symmetrical structure and bonds with three adjacent molecules [42]. In this article, we mainly study the 2D organic topological insulators  $T(\text{C}_6\text{H}_5)_3$  ( $T = \text{V}, \text{Mn}, \text{Fe}, \text{Tc}, \text{Re}$ ), which provide a certain basis for the synthesis of 2D organic topological insulators in experiments.

## 2. Calculation method

All first-principles calculations were performed by using the Vienna *ab initio* simulation package (VASP) [43]. The plane-wave cutoff energy was set to 500 eV. The electronic-exchange correlation interactions were treated by generalized gradient approximation (GGA) of the Perdew–Burke–Ernzerhof (PBE) [44]. The  $k$ -point mesh of  $7 \times 7 \times 1$  was used to sample the Brillouin zone. We used the Wannier90 package to get the tight-binding model, which was based on maximally localized Wannier functions (MLWF) method. We used the Wannier–Tools package [45] to calculate the topological surface states by using the Green function [46]. The formation energy ( $E_{\text{formation}}$ ) was defined as:

$$E_{\text{formation}} = E_{\text{total}} - N_1 E_T - N_2 E_C - N_3 E_H, \quad (1)$$

where  $N_i$  is the number of atoms in one  $T(\text{C}_6\text{H}_5)_3$  primitive cell,  $E_{\text{total}}$  is the total energy of the primitive cell,  $E_T$  is the energy of single transition metal ( $T = \text{V}, \text{Mn}, \text{Fe}, \text{Tc}, \text{Re}$ ) atom,  $E_C$  is the energy of single carbon atom,  $E_H$  is the energy of single hydrogen atom, and  $E_{\text{total}}$  represents the total energy of a single organic molecule after optimization.  $N_1, N_2, N_3$  represents the number of transition metal, carbon, and hydrogen atoms in the primitive cell, respectively.

## 3. Results and discussion

The organic materials  $T(\text{C}_6\text{H}_5)_3$  ( $T = \text{V}, \text{Mn}, \text{Fe}, \text{Tc}, \text{Re}$ ) have the same crystal (space group  $P\bar{3}$ , No. 147) and electronic structure, so we mainly show the results of Fe  $(\text{C}_6\text{H}_5)_3$  in this paper. The Fe  $(\text{C}_6\text{H}_5)_3$  molecule is composed of a Fe atom and three benzene rings, with threefold rotational symmetry, as shown in Fig. 1. The optimized lattice constants are  $a = b = 10.727 \text{ \AA}$ , with the vacuum layer  $c = 20 \text{ \AA}$ . The distance between two adjacent Fe atoms is  $6.467 \text{ \AA}$  and the height of the sandwich is  $1.862 \text{ \AA}$ . Every Fe atom in the whole structure is connected by three benzene rings.

We first calculated the formation energies of the five kinds of materials and got the formation energy of  $T(\text{C}_6\text{H}_5)_3$  as  $-206.82, -203.64, -206.19, -209.63,$  and  $-209.98 \text{ eV}$  for  $T = \text{V}, \text{Mn}, \text{Fe}, \text{Tc}, \text{Re}$ , respectively. The larger negative formation energy indicates that these

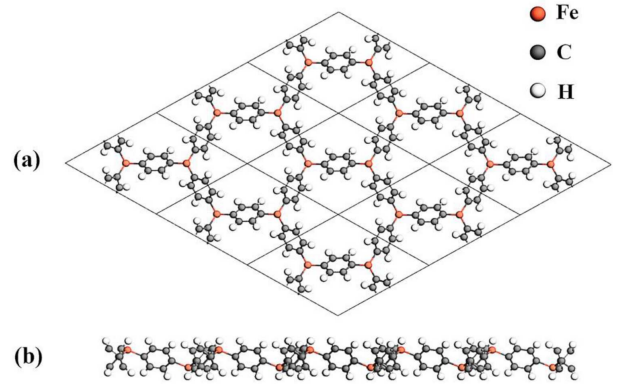


Fig. 1. (a) Top and (b) side view of 2D organic material  $\text{Fe}_2\text{C}_{18}\text{H}_{12}$ .

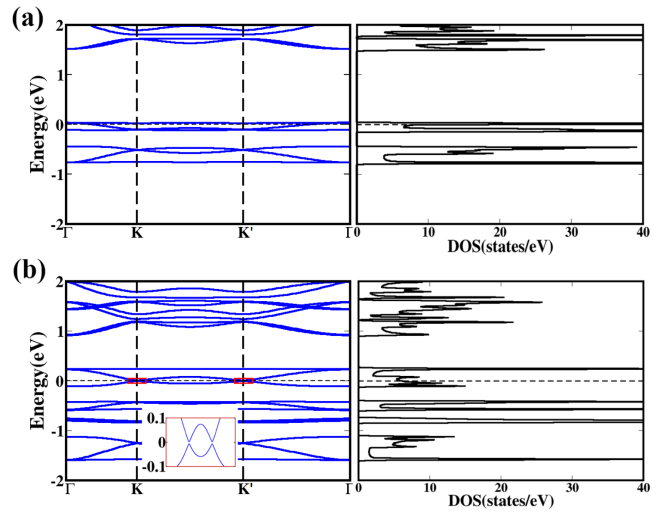


Fig. 2. The band structures of  $\text{Fe}_2\text{C}_{18}\text{H}_{12}$ (a) without and (b) with SOC, respectively. The band structures around the two crossing points are zoomed-in by the inserted figures, in the red rectangles. The density of states of  $\text{Fe}_2\text{C}_{18}\text{H}_{12}$  without and with SOC, respectively.

2D materials can be synthesized. From the formation energy, we find that  $\text{Re}_2\text{C}_{18}\text{H}_{12}$  is easiest to be synthesized, and  $\text{Mn}_2\text{C}_{18}\text{H}_{12}$  is the hardest one to be synthesized.

In this paper, we will take  $\text{Fe}_2\text{C}_{18}\text{H}_{12}$  as an example. We first calculated the band structure of the  $\text{Fe}_2\text{C}_{18}\text{H}_{12}$  without SOC in the nonmagnetic state, as shown in Fig. 2a. Without SOC, there are two Dirac points at  $K$  and  $K'$  points. When SOC is included, the band gap opened at previous gapless points  $K$  and  $K'$ , indicating the topological insulator induced by the SOC, in Fig. 2b. In the presence of SOC, breaking of the spin-rotation symmetry will cause the occurrence of the Dirac cone broken. Next, we can find that the band structure of  $\text{Fe}_2\text{C}_{18}\text{H}_{12}$  opens a band gap of  $8.6 \text{ meV}$  near the Fermi level, as shown in Fig. 2b. The energy gap of  $T(\text{C}_6\text{H}_5)_3$  ( $T = \text{V}, \text{Mn}, \text{Tc}, \text{Re}$ ) are  $3.8, 6.6, 25,$  and  $104.8 \text{ meV}$ , respectively, when SOC is included.

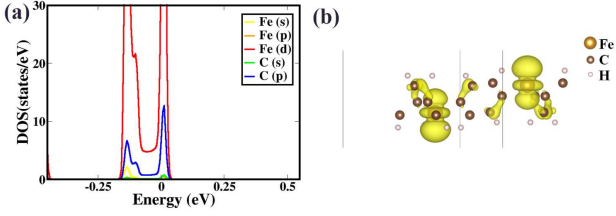


Fig. 3. (a) Partial density of states of Fe and C atoms around the Fermi level. (b) The partial charge density of  $\text{Fe}_2\text{C}_{18}\text{H}_{12}$  near the Fermi level.

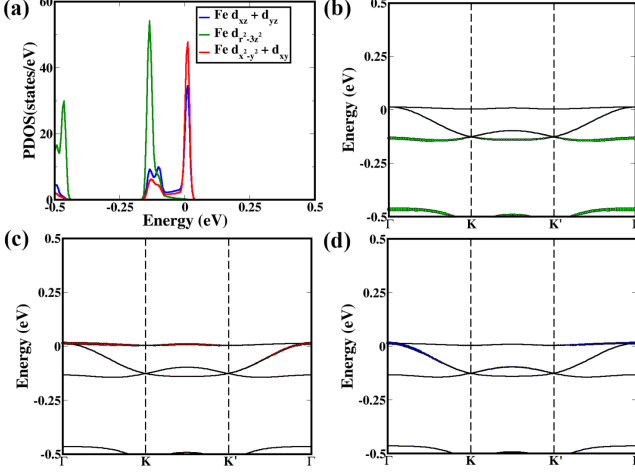


Fig. 4. (a) Partial density of states of Fe  $d$  orbitals. The projected band structure of (b)  $d_{r^2-3z^2}$ , (c)  $d_{x^2-y^2} + d_{xy}$ , (d)  $d_{xz} + d_{yz}$ . The circle sizes correspond to the weights of Fe  $d$  orbitals states.

We show the partial density of states of Fe and C atoms around the Fermi level in Fig. 3a. We can clearly see that around the Fermi level the states are mainly derived from Fe  $3d$  states, with some hybridization of C  $2p$  states. In order to reveal which band forms the Dirac points in Fig. 2a, we plot the charge density near the Fermi level in Fig. 3b. From the charge densities, we know that the Dirac points are mainly derived from the Fe  $d_{r^2-3z^2}$  state, with very small hybridization from C  $2p$  states. The partial density of states and projected band structure are presented in Fig. 4a–d. Above the Fermi level, the flat band is mainly derived from the  $d_{yz}$  and  $d_{x^2-y^2}$  orbitals, while the Dirac bands mainly come from the  $d_{r^2-3z^2}$  band, consistent with the charge densities in Fig. 3b.

In the nonmagnetic state, as shown in Fig. 2a, the flat band and the large DOS around Fermi level imply the magnetic instability according to the Stoner criteria [47]. For the nonmagnetic state, the DOS at the Fermi level  $N(E_f)$  is 12.6 state/eV per Fe atom. The Stoner parameter of Fe atom  $I^{\text{Fe}}$  is 0.9 [48], resulting in  $N(E_f)I^{\text{Fe}} \gg 1$ . Therefore, the nonmagnetic state is unstable, and it will converge to the ferromagnetic state, which is also confirmed by the total energies. In the  $\text{Fe}_2\text{C}_{18}\text{H}_{12}$ , the

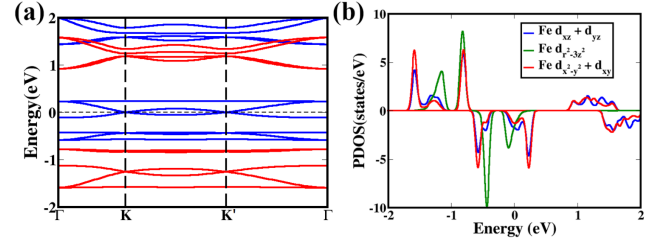


Fig. 5. (a) The band structure of ferromagnetic state of  $\text{Fe}_2\text{C}_{18}\text{H}_{12}$ . Red lines and blue lines denote spin-up and spin-down bands. (b) The partial density of states of Fe  $d$  orbitals.

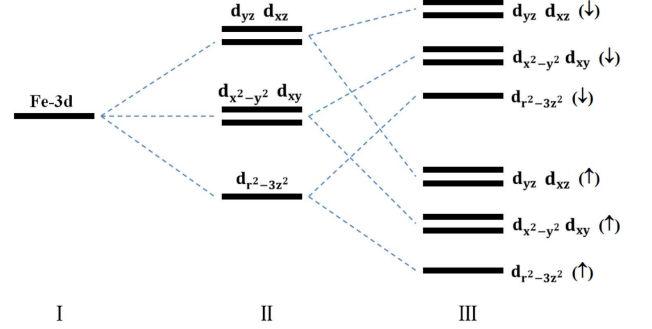


Fig. 6. The energy level diagrams of the Fe  $3d$  orbitals. (I) Chemical bonding, (II) hexagonal crystal field (CF), (III) exchange field.

Fe atom is the center of the triangle formed by three C atoms. There are electron transfers between Fe and C atoms. Results from our calculation results indicate that there are 6.9 electrons around Fe atom. Comparing with the isolated Fe atom configuration  $3d^6 4s^2$ , we find 1.1 electrons per Fe translated to C  $2p$  state. Such electrons transfer cannot form closed C  $2p$ -shell. Therefore, the chemical bonds between Fe and C atoms should have both ionic and covalent characters. The magnetic moments of Fe and C atoms are about  $1.1 \mu_B$  and  $0.1 \mu_B$ , respectively. The molecular dynamics simulation showed that the antiferromagnetic configuration of  $\text{Fe}_2\text{C}_{18}\text{H}_{12}$  is unstable [39]. The total energy of ferromagnetic state is 0.46 eV lower than that of the nonmagnetic state. At the Fermi level, the bands and DOS only come from the spin-down states, with the spin-up states being gapped, which indicates the compound is half-metal. Therefore, we calculated the band structure and DOS of ferromagnetic state shown in Fig. 5.

The Fermi level will move downwards when considering the magnetic state, and the Dirac point just falls at the Fermi level, as shown in Fig. 5a. Red lines and blue lines denote spin-up and spin-down bands, and only the spin-down band is left around the Fermi level. This is caused by electron spin exchange split. In this material, the Fe atoms are triangle liganded by the C atoms in the  $xy$ -plane, without ligand atom along

TABLE I

The energy of NM, FM and AF states (in eV).

	NM	FM	AFM
$V_2C_{18}H_{12}$	-214.99	-216.11	-215.91
$Mn_2C_{18}H_{12}$	-214.94	-216.90	-215.75
$Tc_2C_{18}H_{12}$	-217.21	-217.34	-217.24
$Re_2C_{18}H_{12}$	-220.24	-220.25	-220.22

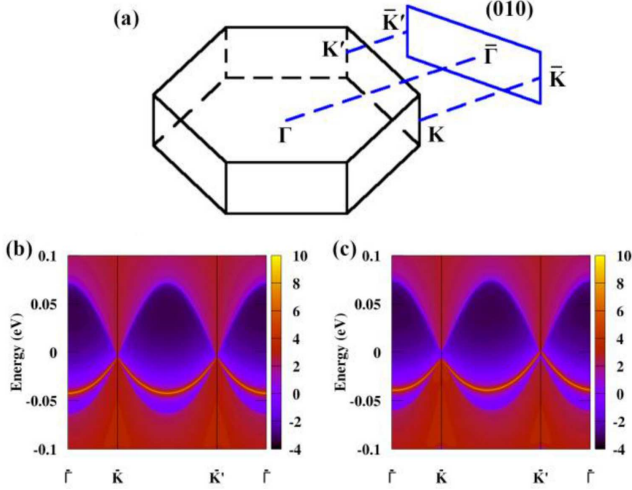


Fig. 7. (a) Brillouin zone and the projected surface Brillouin zones of (010) plane, as well as high-symmetry points. The surface states (a) without SOC and (b) with SOC in the (010) direction.

$z$ -axis. Therefore, the degenerated  $3d$  orbitals split as  $d_{r^2-3z^2} < d_{x^2-y^2}(d_{xy}) < d_{yz}(d_{xz})$ . We have made the energy level diagrams of the Fe  $3d$  orbitals in three states (see Fig. 6). The sign ( $\uparrow$ ) represents the spin-up electrons in the  $d$  orbitals. The sign ( $\downarrow$ ) represents the spin-down electrons in the  $d$  orbitals. In the exchange field, the order of spin-up and spin-down electrons filling energy levels is the same as that in the hexagonal crystal-field. In this paper, the changes of T ( $T = V, Mn, Fe, Tc, Re$ ) atoms have no effect on the crystal field splitting, but the hybridisation between C  $p$  orbitals and T  $d$  orbitals is important [49].

In order to determine the true ground state, we have considered three different magnetic cases. These are non-magnetic (NM), ferromagnetic (FM), and antiferromagnetic (AFM) states. The AFM configuration is constructed in this paper, where the two nearest neighbor spins of Fe atoms are antiparallel with each other. In order to determine the true ground state, we calculated the total energies of three different magnetic states, such as NM, FM, AFM, in Table I. We can see the ground states of  $T(C_6H_5)_3$  ( $T = V, Mn, Tc, Re$ ) are FM, FM, FM, respectively.

In order to study the topological properties of  $Fe_2C_{18}H_{12}$ , we plotted the surface states which projected onto the (010) plane in Fig. 7. Without SOC, the surface

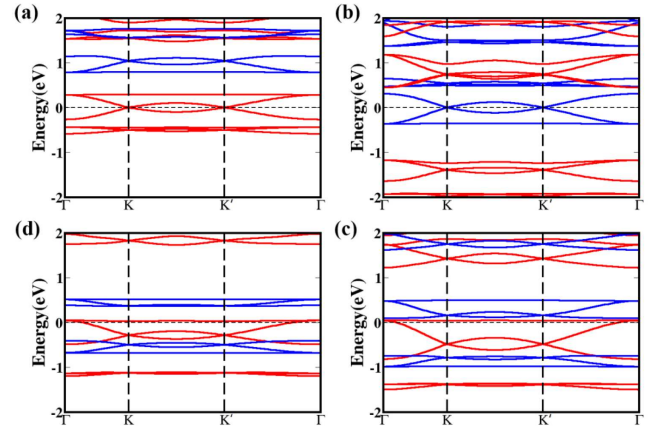


Fig. 8. The band structure of (a)  $V_2C_{18}H_{12}$ , (b)  $Mn_2C_{18}H_{12}$ , (c)  $Tc_2C_{18}H_{12}$ , (d)  $Re_2C_{18}H_{12}$  without SOC. Red lines and blue lines denote spin-up and spin-down bands.

states show typical Dirac points at  $K$  and  $K'$  in Fig. 7b. This Dirac half-metallic state is protected by  $C_3$  rotational symmetry. In the presence of SOC, the Dirac cone must be destroyed due to the spin-rotation symmetry breaking, and then the Dirac half-metallic state converts into the QAH insulating state. Topological insulators are generally protected by time reversal symmetry. If magnetic atoms are introduced, the time reversal symmetry will be broken, resulting in the chiral edge state at the material boundary. When we included SOC, the surface states show topological character, with surface states connecting conduction and valence bands in the bulk band gap, as shown in Fig. 7c. The bulk bands gap is about 0.12 meV, which means that it can be measured at room temperature.

As the five organic materials have the same crystal and electronic structures, we speculate that they have similar bands structures and topological properties in Fig. 8, we show the band structures of  $V_2C_{18}H_{12}$ ,  $Mn_2C_{18}H_{12}$ ,  $Tc_2C_{18}H_{12}$ ,  $Re_2C_{18}H_{12}$ , respectively. The band structures of  $V_2C_{18}H_{12}$  and  $Mn_2C_{18}H_{12}$  show linear band crossing with Dirac point at the  $K$  and  $K'$  points around Fermi level. The linear band crossing points (at  $K$  and  $K'$ ) of  $Tc_2C_{18}H_{12}$ ,  $Re_2C_{18}H_{12}$  are about 0.5 eV below the Fermi level.

#### 4. Conclusion

We studied the topological properties of the 2D organic material  $T(C_6H_5)_3$  ( $T = V, Mn, Fe, Tc, Re$ ) by using the first-principles calculation. All the compounds are the Dirac semimetal without SOC and spin polarization. They change to topological insulators when the spin polarization and SOC are included. Such 2D organic topological insulators with the chiral edge states are the best system to achieve the QAHE. These compounds will provide a platform to achieve the application of QAHE in semiconductors, solar cells, and integrated circuit.

### Acknowledgments

We thank the Foundation Key Scientific Research Project of Universities in Henan Province (No. 19zx008). We also thank the High Performance Computing Center (HPC) of Henan Normal University for providing high performance computation.

### References

- [1] F.D.M. Haldane, *Phys. Rev. Lett.* **61**, 2015 (1988).
- [2] B.A. Bernevig, T.L. Hughes, S. Zhang, *Science* **314**, 1757 (2006).
- [3] M. König, S. Wiedmann, C. Brüne, A. Roth, H. Buhmann, L.W. Molenkamp, X. Qi, S. Zhang, *Science* **318**, 766 (2007).
- [4] A. Roth, C. Brüne, H. Buhmann, L.W. Molenkamp, J. Maciejko, X. Qi, S. Zhang, *Science* **325**, 294 (2009).
- [5] C. Brune, A. Roth, H. Buhmann, E.M. Hankiewicz, L.W. Molenkamp, J. Maciejko, X. Qi, S. Zhang, *Nat. Phys.* **8**, 485 (2012).
- [6] R. Yu, W. Zhang, H. Zhang, S. Zhang, X. Dai, Z. Fang, *Science* **329**, 61 (2010).
- [7] C. Chang, J. Zhang, M. Liu et al., *Adv. Mater.* **25**, 1065 (2013).
- [8] K.S. Novoselov, A.K. Geim, S.V. Morozov, D. Jiang, Y. Zhang, S.V. Dubonos, I.V. Grigorieva, A.A. Firsov, *Science* **306**, 666 (2004).
- [9] Z. Qiao, S.A. Yang, W. Feng, W.K. Tse, J. Ding, Y. Yao, *Phys. Rev. B* **82**, 161414 (2010).
- [10] Z. Qiao, W. Ren, H. Chen, L. Bellaiche, Z. Zhang, A.H. MacDonald, Q. Niu, *Phys. Rev. Lett.* **112**, 116404(2014).
- [11] H. Wang, W. Luo, H. Xiang, *Phys. Rev. B* **95**, 125430 (2017).
- [12] S. Zhang, C. Zhang, S. Zhang, W. Ji, P. Li, P. Wang, S. Li, S. Yan, *Phys. Rev. B* **96**, 205433 (2017).
- [13] Z. Zanolli, C. Niu, G. Bihlmayer, Y. Mokrousov, P. Mavropoulos, M.J. Verstraete, S. Blugel, *Phys. Rev. B* **98**, 155404 (2018).
- [14] C. Huang, J. Zhou, H. Wu, K. Deng, P. Jena, E. Kan, *Phys. Rev. B* **95**, 045113 (2017).
- [15] W. Zhang, Y. Li, H. Jin, Y. She, *Phys. Chem. Chem. Phys.* **21**, 17740 (2019).
- [16] G. Xu, B. Lian, S. Zhang, *Phys. Rev. Lett.* **115**, 186802 (2015).
- [17] L. Dong, Y. Kim, D. Er, A.M. Rappe, V.B. Shenoy, *Phys. Rev. Lett.* **116**, 096601 (2016).
- [18] M. Zhao, W. Dong, A. Wang, *Sci. Rep.* **3**, 3532 (2013).
- [19] Z. Liu, Z. Wang, J. Mei, Y. Wu, F. Liu, *Phys. Rev. Lett.* **110**, 106804 (2013).
- [20] J. Sakamoto, J. van Heijst, O. Lukin, A.D. Schluter, *Angew. Chem. Int. Ed.* **48**, 1030 (2009).
- [21] T. Classen, G. Fratesi, G. Costantini, S. Fabris, F.L. Stadler, C. Kim, S. Gironcoli, S. Baroni, K. Kern, *Angew. Chem. Int. Ed.* **44**, 6142 (2005).
- [22] S. Uji, H. Shinagawa, T. Terashima, T. Yakabe, Y. Terai, M. Tokumoto, A. Kobayashi, H. Tanaka, H. Kobayashi, *Nature* **410**, 908 (2001).
- [23] C. Adachi, K. Nagai, N. Tamoto, *Appl. Phys. Lett.* **66**, 2679 (1995).
- [24] Y. Cui, H. Yao, B. Gao, Y. Qin, S. Zhang, B. Yang, C. He, B. Xu, J. Hou, *J. Am. Chem. Soc.* **139**, 7302 (2017).
- [25] M. Muccini, *Nat. Mater.* **5**, 605 (2006).
- [26] P. Horcajada, R. Gref, T. Baati, P.K. Allan, G. Maurin, P. Couvreur, G. Ferey, R.E. Morris, C. Serre, *Chem. Rev.* **112**, 1232 (2011).
- [27] Q. Yang, Q. Xu, H. Jiang, *Chem. Soc. Rev.* **46**, 4774 (2017).
- [28] P. Horcajada, T. Chalati, C. Serre, et al., *Nat. Mater.* **9**, 172 (2010).
- [29] L.J. Murray, M. Dinca, J.R. Long, *Chem. Soc. Rev.* **38**, 1294 (2009).
- [30] C. Chang, J. Zhang, X. Feng, et al., *Science* **340**, 167 (2013).
- [31] J.G. Checkelsky, R. Yoshimi, A. Tsukazaki, K.S. Takahashi, Y. Kozuka, J. Falson, M. Kawasaki, Y. Tokura, *Nat. Phys.* **10**, 731 (2014).
- [32] X. Kou, Y. Fan, M. Lang, P. Upadhyaya, K.L. Wang, *Solid State Commun.* **215**, 34 (2015).
- [33] Y. Ma, Y. Dai, X. Li, Q. Sun, B. Huang, *Carbon* **73**, 382 (2014).
- [34] Z. Wang, Z. Liu, F. Liu, *Nat. Commun.* **4**, 1471(2013).
- [35] H. Huang, Z. Liu, H. Zhang, W. Duan, D. Vanderbilt, *Phys. Rev. B* **92**, 161115 (2015).
- [36] Y. Jin, Z. Chen, B. Xia, Y. Zhao, R. Wang, H. Xu, *Phys. Rev. B* **98**, 245127 (2018).
- [37] Z. Shi, J. Liu, T. Lin, F. Xia, P. Liu, N. Lin, *J. Am. Chem. Soc.* **133**, 6150 (2011).
- [38] L. Kou, Y. Ma, Z. Sun, T. Heine, C. Chen, *J. Phys. Chem. Lett.* **8**, 1905 (2017).
- [39] H. Hu, Z. Wang, F. Liu, *Nanoscale Res. Lett.* **9**, 690 (2014).
- [40] Y. Ren, Z. Qiao, Q. Niu, *Rep. Prog. Phys.* **79**, 066501 (2016).
- [41] U. Schlickum, R. Decker, F. Klappenberger et al., *Nano Lett.* **7**, 3813 (2007).
- [42] Z. Liu, Z. Wang, J. Mei, Y. Wu, F. Liu, *Phys. Rev. Lett.* **110**, 106804 (2013).
- [43] D. Kan, X. Zhang, Y. Zhang, Z. Yang, *J. Power Sources* **378**, 691 (2018).
- [44] F. Shang, G. Wang, *Comp. Mater. Sci.* **160**, 275 (2019).
- [45] Z. Wang, G. Wang, X. Shi, D. Wang, X. Tian, *J. Phys. D Appl. Phys.* **50**, 465304 (2017).
- [46] M. Zhang, G. Wang, *Comput. Mater. Sci.* **171**, 109206 (2020).
- [47] E.C. Stoner, *Proc. R. Soc. Lond.* **165**, 372 (1938).
- [48] J.F. Janak, *Phys. Rev. B* **16**, 255(1977).
- [49] C. Autieri, A. Bouhon, B. Sanyal, *Philos. Mag.* **97**, 3381 (2017).